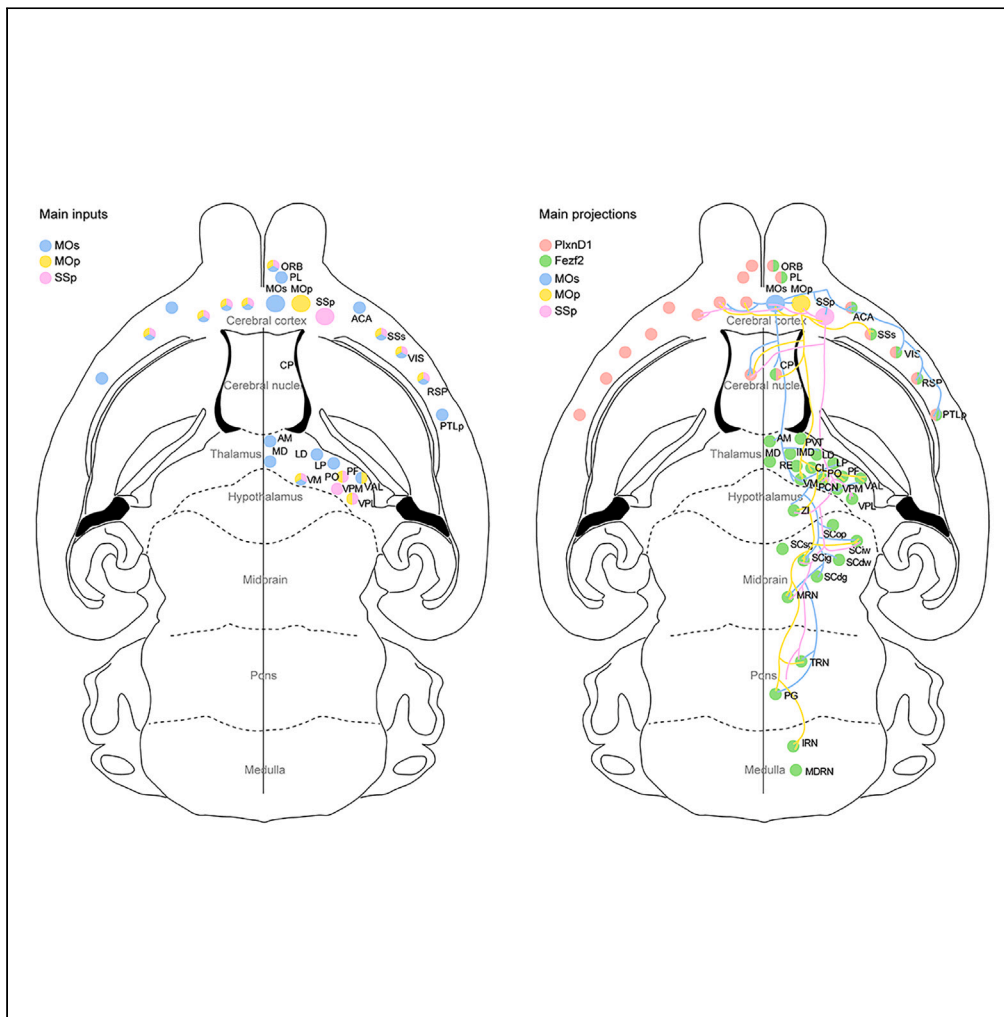


Article

# Long-range connectome of pyramidal neurons in the sensorimotor cortex



Mei Yao,  
Ayizuohere Tudi,  
Tao Jiang, ..., Z.  
Josh Huang, Hui  
Gong, Xiangning  
Li

lixiangning@mail.hust.edu.cn

**Highlights**

Systematically mapped the whole-brain connections in six cortical subregions

IT and PT neurons in the same subregion received from a similar circuit

Different subregions received from the preferred neuron populations

The cortical and thalamic connections showed topological correspondence

Yao et al., iScience 26, 106316  
April 21, 2023 © 2023  
<https://doi.org/10.1016/j.isci.2023.106316>



## Article

## Long-range connectome of pyramidal neurons in the sensorimotor cortex

Mei Yao,<sup>1,4</sup> Ayizuohere Tudi,<sup>1,4</sup> Tao Jiang,<sup>2</sup> Xu An,<sup>3</sup> Qingtao Sun,<sup>1</sup> Anan Li,<sup>1,2</sup> Z. Josh Huang,<sup>3</sup> Hui Gong,<sup>1,2</sup> and Xiangning Li<sup>1,2,5,\*</sup>

## SUMMARY

The neocortex mediates information processing through highly organized circuitry that contains various neuron types. Distinct populations of projection neurons in different cortical regions and layers make specific connections and participate in distinct physiological functions. Herein, with the fluorescence micro-optical sectioning tomography (fMOST) and transgenic mice that targeted intratelencephalic (IT) and pyramidal tract (PT) neurons at specific layers, we dissected the long-range connectome of pyramidal neurons in six subregions of the sensorimotor cortex. The distribution of the input neurons indicated that IT and PT neurons in the same region received information from similar regions, while the neurons in different subregions received from the preferred neuron populations. Both the input and projection areas of these six subregions showed the transverse and longitudinal correspondence in the cortico-cortical, cortico-thalamic, and cortico-striatal circuits, which indicated that the connections were topologically organized. This study provides a comprehensive resource on the anatomical connections of cortical circuits.

## INTRODUCTION

The mammalian brain processes complex information through various neuronal circuits across cortical and subcortical regions.<sup>1</sup> The neocortex comprises dozens of cortical areas, each consisting of hundreds of neuron types and their local and long-range connections. As the center for sensory information processing and the control of motor action, the sensorimotor cortex is the basis of voluntary movement.<sup>2</sup> Based on the cytoarchitecture, physiology, and histochemistry, the sensorimotor cortex can be divided into different functional regions,<sup>3</sup> such as the primary and secondary motor and sensory cortices. With various demarcation methods, these cortical sectors can be further grouped into different subregions such as the forelimb area expanding into a large space covering the anterior-medial motor area of secondary motor area (MOs<sup>AMM</sup>),<sup>4,5</sup> to the upper limb area of primary somatosensory cortex (SSp-ul).<sup>6,7</sup>

At the macroscopic scale, neuroimaging and physiological investigations have shown that the sensorimotor cortex is topographically organized and that nearby locations represent similar functions. The functional organization depends on the complex circuit structure, while several recent studies have revealed regional and cell-type preference in different circuits.<sup>8–11</sup> Even in the same subregion, different types of neurons such as IT and PT neurons share similar inputs,<sup>9</sup> they participate in different roles in motor control and learning via distinct downstream circuits. The projection targets of PT neurons in the sensorimotor cortex are scattered, including the striatum, thalamus, hypothalamus, midbrain, and other deep nuclei.<sup>8</sup> IT neurons project extensively to multiple regions within the bilateral telencephalon, especially the adjacent cortical regions and striatum, and participate in the preparation and planning of forelimb movements.<sup>9,12</sup> The same type of neuron in different layers also can involve in different functional regulations through preferred connection patterns. For example, PT neurons of superficial layers in MOp<sup>ALM</sup> project to the thalamus and participate in planning activities, while deep layer neurons project to the pre-motor center of the spinal cord and play a key role in the motor execution stage of the lever pressing task.<sup>13</sup> These validated the uniqueness of the medulla projection in MOp<sup>ALM</sup>, as opposed to the extensive projection properties of MOp, indicating the importance of cross-regional anatomy of specific cell types.<sup>13</sup> Similarly, although previous studies indicated IT neurons convey planning information to striatum, IT neurons in different regions or layers of the sensorimotor cortex prefer to participate in different roles

<sup>1</sup>Britton Chance Center for Biomedical Photonics, Wuhan National Laboratory for Optoelectronics, MoE Key Laboratory for Biomedical Photonics, Huazhong University of Science and Technology, Wuhan, China

<sup>2</sup>Research Unit of Multimodal Cross Scale Neural Signal Detection and Imaging, Chinese Academy of Medical Sciences, HUST-Suzhou Institute for Brainistics, JITRI, Suzhou, China

<sup>3</sup>Department of Neurobiology, Duke University Medical Center, Durham, NC, USA

<sup>4</sup>These authors contributed equally

<sup>5</sup>Lead contact

\*Correspondence: [lixiangning@mail.hust.edu.cn](mailto:lixiangning@mail.hust.edu.cn)  
<https://doi.org/10.1016/j.isci.2023.106316>



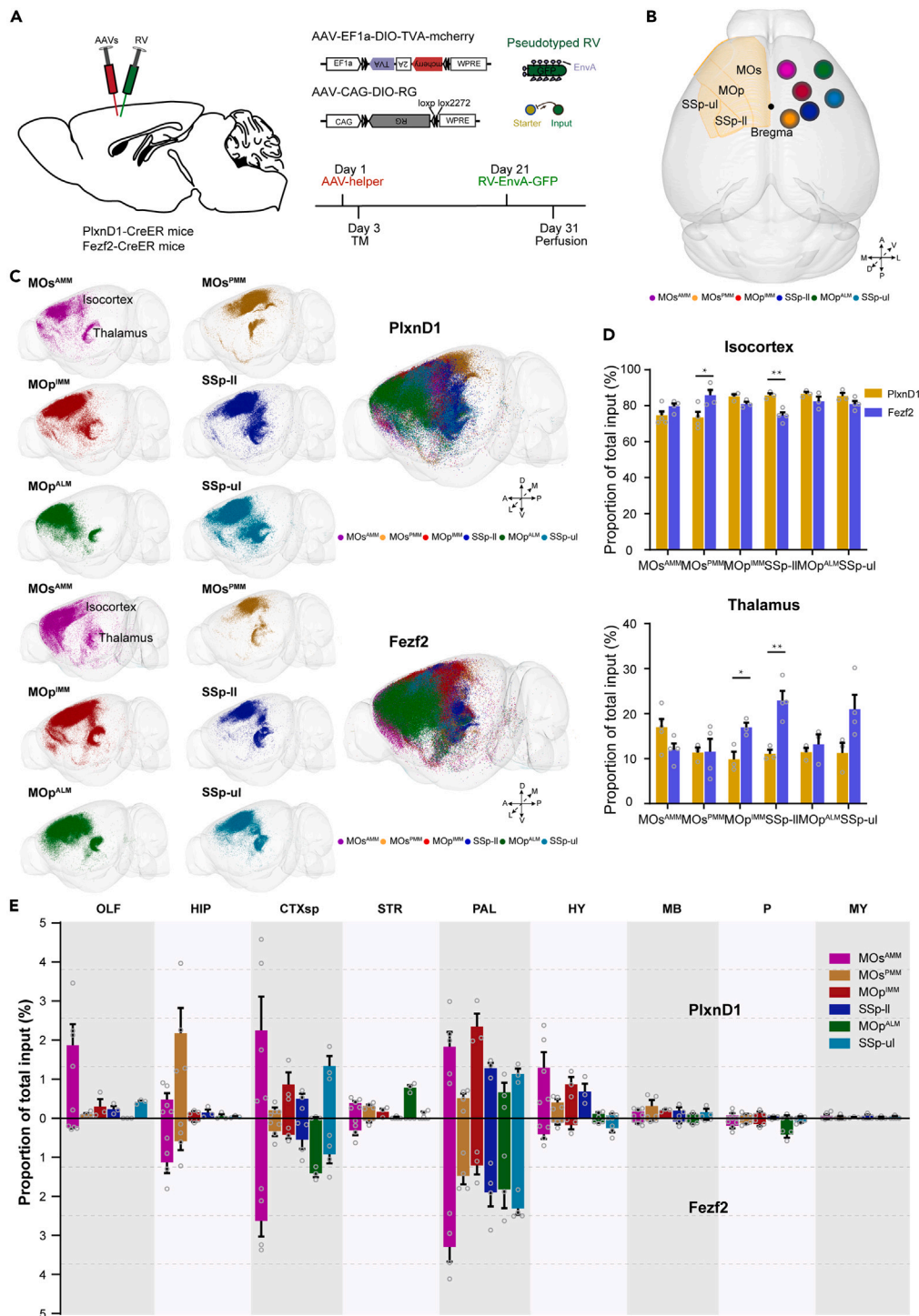


**Figure 1. Whole-brain input to cortical pyramidal neurons**

(A) The labeling strategy of the whole-brain inputs to type-specific neurons.

(B) Different injection sites of the sensorimotor cortex. The left hemispheres showed the three-dimensional distribution of different regions of the sensorimotor cortex, while the right hemispheres showed the actual injection sites.

(C) Three-dimensional display of whole-brain input neuron of pyramidal neurons in different subregions. Each point represented one neuron. Different colors represented different subregions. The three-dimensional direction of the mouse brain outline was displayed. The somata of RV-labeled neurons was extracted by NeuroGPS and registered to the CCF.

**Figure 1. Continued**

(D) Quantitative analysis and comparison of the cortical and thalamic input of pyramidal neurons. The vertical axis of the histogram represented the percentage of input neurons in the cortex and thalamus of the whole brain. The two-tailed Student's *t* test was used to compare the input strength between different subregions. \**p* < 0.05, \*\**p* < 0.01. Data were represented as mean ± SEM.

(E) Quantitative analysis and comparison of input from whole-brain except for the cortex and thalamus. One-way ANOVA followed by Tukey's post hoc tests. Data were represented as mean ± SEM. The abbreviations of brain regions were provided in Table S1. The significant difference in input intensity in different subregions was compared, and the *p* values were shown in Tables S2–S4.

with corresponding anatomical connections.<sup>14,15</sup> IT neurons of MOs<sup>AMM</sup> show strong target location selectivity.<sup>14</sup> IT neurons in layer 2/3 of MOp<sup>IMM</sup> are responsible for monitoring the results of the success of grasping food,<sup>15</sup> while IT neurons in layer 2/3 of MOp<sup>ALM</sup> and MOs<sup>PMM</sup> are involved in licking control.<sup>16</sup> In addition, both IT and PT neurons of MOp<sup>IMM</sup> play an important role in motor control.<sup>17,18</sup> To sum up, these differences may depend on regions and cell types, further illustrating the need to explore detailed anatomical connection differences. To clarify the organizational rules underlying their distinct roles in movements, it is necessary to analyze their input and projection circuits in the whole brain. Previous studies have shown that the sensorimotor cortex integrates inputs from multiple regions including the cortex and subcortical areas, and transmits information by the long-range projections to multiple downstream regions.<sup>10,19,20</sup> These studies reveal the difficulty in understanding the organizational logic of the cortex and offering a unique perspective on complex functions.<sup>10,21</sup>

In this study, combining anterograde tracing,<sup>9,10</sup> rabies virus retrograde labeling,<sup>22–26</sup> and fluorescence micro-optical sectioning tomography (fMOST),<sup>27</sup> we derived a comprehensive anatomical resource at the circuit level for the mouse sensorimotor cortex and investigated the connectome of IT and PT neurons in six cortical subregions. These results revealed the connectivity patterns of pyramidal neurons in the forelimb sensorimotor cortex, which provides a road map for understanding the functional organization and circuit structure of forelimb movement.

**RESULTS****Whole brain input distribution of different pyramidal neurons in the sensorimotor cortex**

Previous reports have indicated that a variety of genetic molecules can be used to target IT and PT neurons in the cortex, such as *PlxnD1* and *Fezf2*. To obtain the whole-brain input of IT and PT neurons, we performed the retrograde *trans*-synaptic tracing<sup>28</sup> in *PlxnD1*-CreER and *Fezf2*-CreER mice respectively (Figure 1A). We chose six injection sites in the motor and sensor cortices, including the anterior-lateral motor area of the primary motor area (MOp<sup>ALM</sup>), the posterior-medial motor area (MOs<sup>PMM</sup>), MOs<sup>AMM</sup>, the intermediate-medial motor area (MOp<sup>IMM</sup>), SSp-ul, and the lower limb area of the primary somatosensory cortex (SSp-ll). *PlxnD1*+ and *Fezf2*+ neurons were distributed in specific layers in the cortex, located on layers 2/3 and 5a, and layers 5 and 6 respectively (Figures S1A and S1B). These neurons demonstrated the projection pattern of IT and PT neurons respectively.<sup>8,9,29</sup> The starter cells (neurons co-expressing TVA-mCherry and EnvA-GFP) in different subregions were restricted in the injection sites and specific layers (Figures 1B and S1B–S1D), which validates the specificity of the viral tracing system.

To compare the whole-brain input circuits of different subregions, we imaged the brains using the fMOST system with spatial resolution at  $0.32 \times 0.32 \times 2 \mu\text{m}^3$  (Figure S2). Then we obtained the spatial information of all input neurons via neuroGPS<sup>30</sup> software and subsequently registered the datasets to the Allen Mouse Brain Common Coordinate Framework (CCF) (Figure 1C). Quantitative results showed that the majority of the input neurons were detected in the ipsilateral adjacent cortex and contralateral homologous cortex, followed by the lateral and medial thalamus (Figures 1C and S2). Compared to IT neurons, PT neurons in the MOs<sup>PMM</sup> received more input from cortical areas (*p* < 0.01), while the situation is the opposite in the SSp-ll (*p* < 0.05). The PT neurons in the MOp<sup>IMM</sup> (*p* < 0.05) and SSp-ll (*p* < 0.01) received more thalamic input than IT neurons (Figure 1D). In addition to the input from the isocortex and thalamus, these pyramidal neurons widely received input from other areas (Figure 1E), mainly in the cortical subplate and pallidum. The hippocampus sent a significantly higher proportion of input to the MOs<sup>AMM</sup> and MOs<sup>PMM</sup> than to other subregions. Furthermore, the striatum preferentially innervated the MOs<sup>AMM</sup> and the MOp<sup>ALM</sup> rather than other subregions (Figure 1E). Most of the input connections were selective to the specific cell types in the same subregions. The pallidum preferentially sent projections to the PT neurons in the MOs<sup>AMM</sup> (*p* < 0.05), MOs<sup>PMM</sup> (*p* < 0.01), and SSp-ul (*p* < 0.01), while to the IT neurons in the MOp<sup>IMM</sup> (*p* < 0.05) (Figure 1E). In

addition, the olfactory area including the main olfactory bulb, accessory olfactory bulb, and anterior olfactory nucleus sent more input to IT neurons in the  $MOs^{AMM}$  ( $p < 0.05$ ). The striatum sent larger inputs to IT neurons in the  $MOs^{PMM}$  ( $p < 0.01$ ),  $MOp^{ALM}$  ( $p < 0.001$ ), and  $SSp-ul$  ( $p < 0.05$ ). The hypothalamus sent larger inputs to IT neurons in the  $MOs^{PMM}$  ( $p < 0.05$ ) and  $MOp^{IMM}$  ( $p < 0.05$ ) (Figure 1E). These results uncovered that IT and PT neurons of the different cortical regions received biased inputs from multiple brain regions, indicating that the functional differences of pyramidal neurons are contributed by biased inputs.

### Cortical inputs for different types of pyramidal neurons

As a main input region to the sensorimotor cortex, the isocortex held about 80% of input neurons which showed region-preferred patterns (Figures 1D, 1E, and 2A). Interestingly, our results indicated that topological connections that the medial ( $MOs^{AMM}$ ,  $MOs^{PMM}$ ,  $MOp^{IMM}$ , and  $SSp-II$ ) and lateral ( $MOp^{ALM}$  and  $SSp-ul$ ) subregions received input mainly from the medial and lateral cortex respectively. While the anterior ( $MOs^{AMM}$  and  $MOp^{ALM}$ ) and posterior ( $MOp^{PMM}$ ) subregions were innervated by the anterior and posterior cortex respectively (Figure 2B).

These six subregions all received strong input from the motor cortex and primary somatosensory cortex, while some subregions preferred to form a unique connection network with other cortical areas. For example, in the prefrontal cortex, the anterior cingulate area (ACA) preferentially innervated the  $MOs^{AMM}$ ,  $MOs^{PMM}$ , and  $MOp^{IMM}$ , while the prelimbic area (PL) mainly projected to  $MOs^{AMM}$ , and orbital area (ORB) mainly targeted the  $MOs^{AMM}$  and  $MOp^{IMM}$ . The  $SSp-II$ ,  $MOp^{ALM}$ , and  $SSp-ul$  received more input from the supplemental somatosensory area (SSs), while the  $MOs^{PMM}$  received strong input mainly from visual areas (VIS), posterior parietal association areas (PTLp), and retrosplenial area (RSP) (Figure 2C).

We next compared the differences in cortical input patterns between IT and PT neurons in the same subregions. As shown in Figure 2C,  $MOp$  and  $MOs$  preferentially project to the PT neurons of the sensorimotor cortex except for the  $SSp-II$  and  $SSp-ul$ . The PT neurons of  $MOs^{AMM}$  received massive inputs from the medial prefrontal cortex, including PL ( $p < 0.001$ ) and ILA ( $p < 0.001$ ). While ACA provided more projections to the IT neurons than PT neurons in the  $MOs^{AMM}$  ( $p < 0.05$ ). Moreover, the agranular insular cortex (AI) sent more projection to the IT neurons in  $MOp^{IMM}$  ( $p < 0.05$ ),  $SSp-II$  ( $p < 0.05$ ), and  $SSp-ul$  ( $p < 0.001$ ). Together, the cortical connection network of the sensorimotor cortex was organized by region, cell type, and layer specificity, forming complex and diverse sub-circuits.

To further understand layer-specific circuit organization, we compared the layer specificity of cortical input to IT and PT neurons. Our results showed that the cortical input neurons were mainly concentrated in layers 2/3 and 5, and a few of them were found in layer 6, especially for  $MOp^{IMM}$  (Figure 2D). In short, the cortical afferent circuits of the somatic sensorimotor subnetworks were organized in a specific spatial arrangement and contained multiple parallel pathways targeting specific cell types.

### Region-preference of thalamic inputs

The subcortical input neurons were mainly located in the thalamus. The mutual projection between the thalamus and cortex is crucial for the function of cortical neurons.<sup>31</sup> The distribution of input neurons in the thalamic regions for IT and PT neurons in the same subregions were similar (Figures 3A and S3), while the thalamic inputs for different subregions were distinct (Figures 3A and 3B). The  $MOs^{PMM}$  received input mainly from the lateral dorsal nucleus of the thalamus (LD). The other subregions mainly received inputs from the ventrolateral thalamus with regional specificity. The ventral anterior lateral nucleus (VAL) preferentially projected to the  $MOp^{IMM}$  and  $MOp^{ALM}$ , while the ventral posterolateral nucleus (VPL) preferentially innervated the  $SSp-ul$  and  $SSp-II$ . Moreover, the parafascicular nucleus (PF) projected to most regions except the  $MOs^{PMM}$  (Figures 3B and 3C), which indicates that the PF may not involve in associative-sensorimotor functions to modulate motor responses to external stimuli.<sup>32</sup> In addition, compared with other subregions, the  $MOs^{AMM}$  received more inputs from the medial thalamic nucleus (Figures 3B and S3).

Although the input neurons of the IT and PT neurons were distributed in the same thalamic regions, the proportion of inputs in different nuclei showed some differences. The IT neurons of the  $MOs^{PMM}$  received more inputs from LD, compared with the PT neurons (Figure 3C). The VPL preferentially projected to PT neurons of  $SSp-II$ , while the posterior complex of the thalamus (PO) sent richer inputs to IT neurons. In addition, PT neurons in  $MOp^{ALM}$  received stronger input from the intralaminar nuclei of the dorsal thalamus

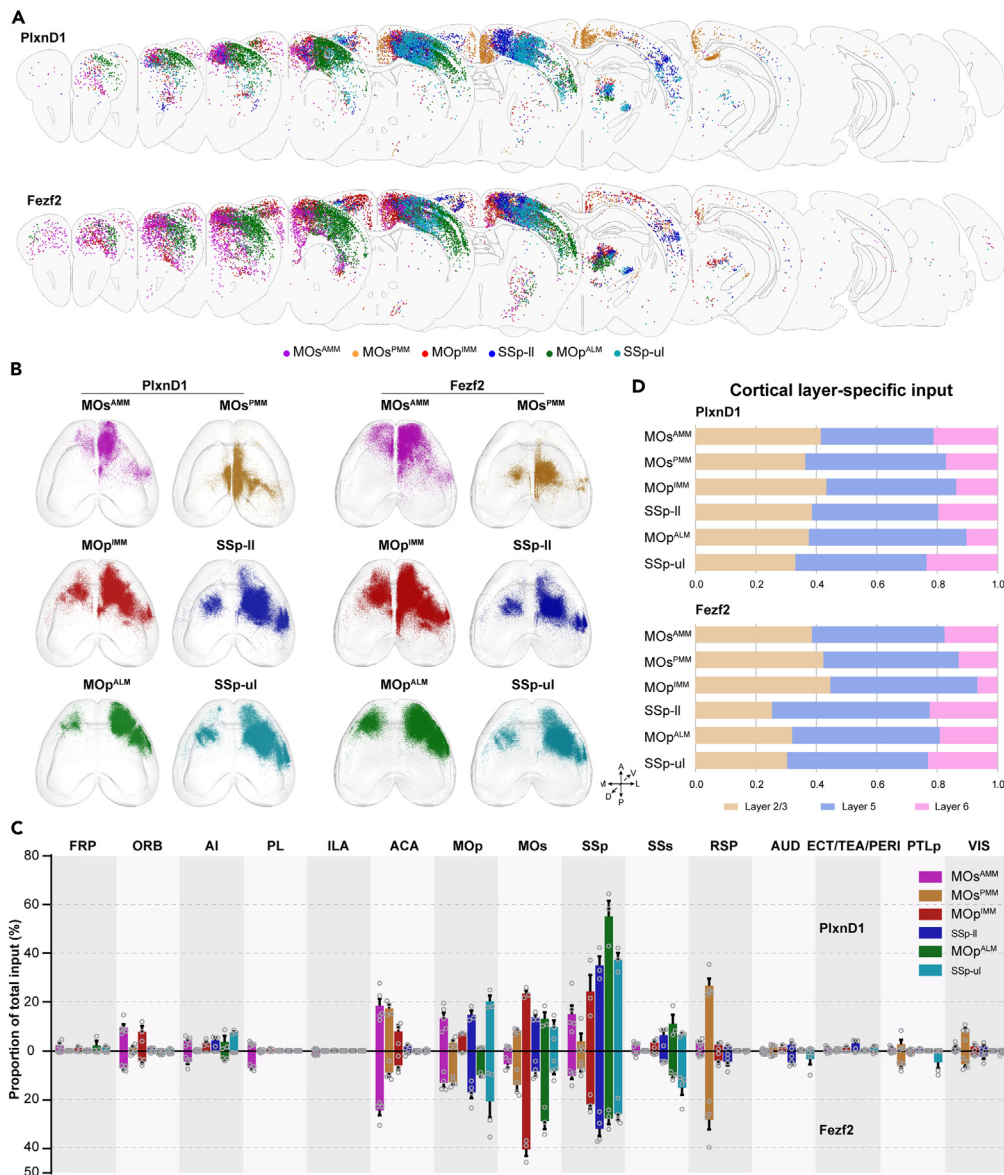


**Figure 2. The monosynaptic input from the isocortex**

(A) Schematic coronal sections depicted the RV-GFP labeled neurons. Each colorful point shows one neuron projecting to the corresponding subregion. The neurons shown in each coronal section (50  $\mu$ m) were derived from a single sample.

(B) Three-dimensional location of the input neuron on the cortex. Each point presented one neuron. The diagram represented the outline of the brain.

(C) Quantitative analysis of input neurons in different subregions of the ipsilateral isocortex. Data were represented as mean  $\pm$  SEM. The significant difference in input intensity in different subregions was compared, and the p values were shown in Tables S2–S4.

(D) Laminar distribution of bilateral cortical input neurons. The ratio of input neurons in each layer of the other cortex to the total input neurons in the layer except the injection site. The numerical value represented the proportion of input neurons in the different layers.

(ILM), while the anterior group of the dorsal thalamus (ATN) provided more input to the IT neurons in SSp-ul (Figures 3C and S3).

In summary, these results suggested that different subregions of the sensorimotor cortex received thalamic input with regional specificity: the ventral group of the dorsal thalamus (VENT) and PO target lateral

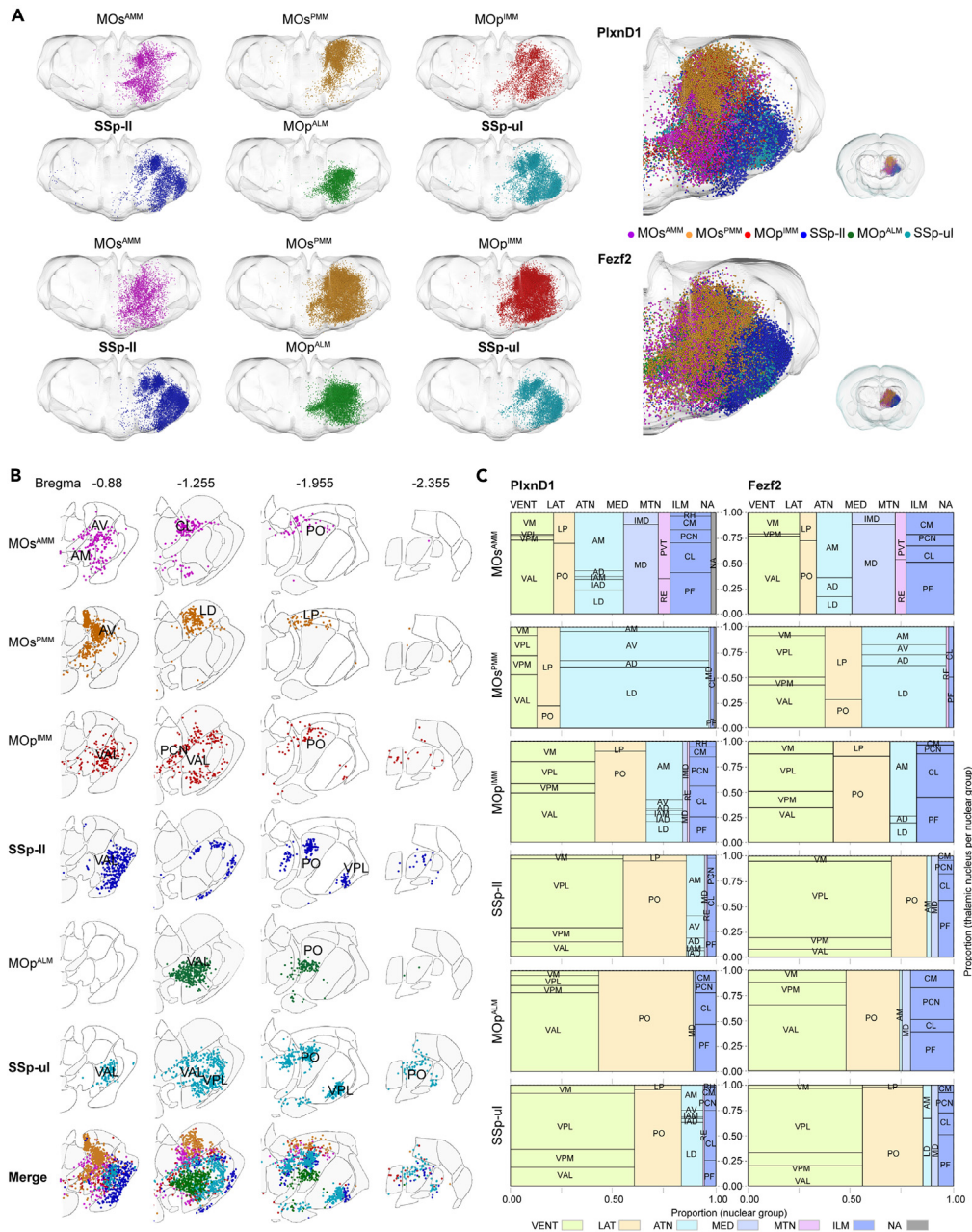


**Figure 3. Region-specific distribution of input neurons in the thalamus**

(A) The front 3D view of input neurons in the thalamus. Each point represented a single input neuron.

(B) The coronal sections of the thalamic inputs to pyramidal neurons in different subregions. The coronal sections of the thalamic inputs to the IT and PT neurons. Along the A-P axis, each group was presented with four coronal sections of thalamic inputs, corresponding to the bregma  $-0.88$  mm,  $-1.255$  mm,  $-1.955$  mm, and  $-2.06$  mm of CCF.

(C) Horizontal axis: the proportion of input within discrete thalamic regions in the different thalamic nuclear groups. Vertical axis: the proportions of input within the thalamic nuclear groups. Different colors represented different thalamic nuclear groups. Different colors represented different layers. The abbreviations of brain regions were provided in [Table S1](#).

subregions; medial thalamus targets medial subregions; dorsolateral thalamic nucleus targets posterior subregions. While the upstream thalamic areas to different layer-specific pyramidal neurons were similar but quantitatively different in some key brain thalamic regions.

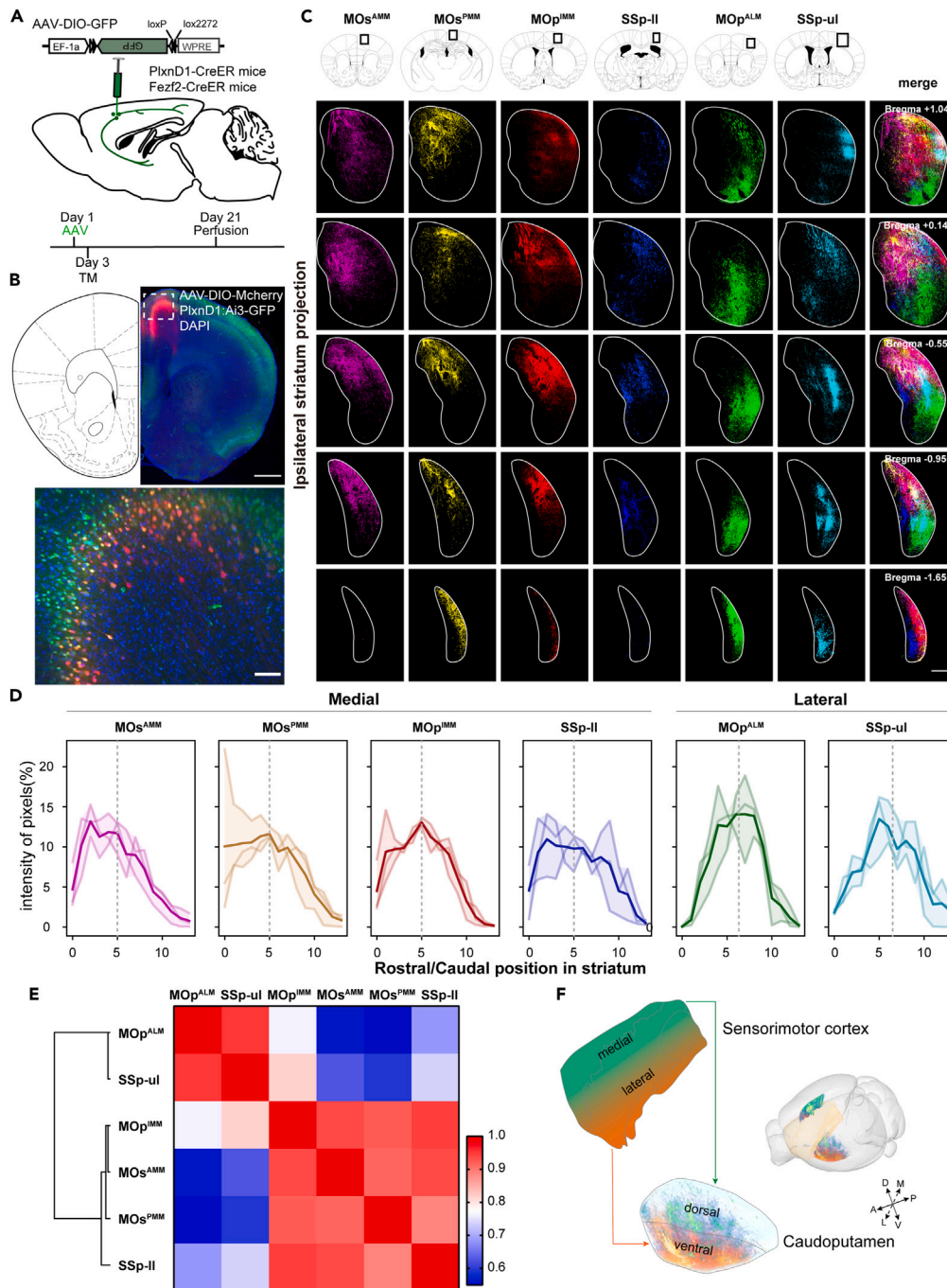


**Figure 4. Topological projections from IT neurons to the striatum**

(A) The labeling strategy of the whole-brain projection from type-specific neurons.

(B) Verify the specificity of labeled neurons. Red: neurons expressing AAV-mcherry, Green: PlxnD1+ neurons, DAPI: signals for the cytoarchitecture. Scale bars: up, 500  $\mu$ m; down, 20  $\mu$ m.

(C) Ipsilateral striatum projection of IT neurons in different subregions. The top row of maps represented the coronal sections of the striatal projection from different subregions, and the box indicated the specific locations of injection sites in CCF. Each column represented a single sample, from top to bottom, showing the topological projection of IT neurons from different subregions to the rostral-caudal striatum. The projection thickness of each image was 100  $\mu$ m. The number below the coronal plane in the first column represented the same position corresponding to CCF. Scale bar = 500  $\mu$ m.

(D) Quantitative analysis of the ipsilateral striatum projection of IT neurons in different subregions. We divided these sites into medial and lateral based on the spatial location of the subregions and compared the projection intensity of the

**Figure 4. Continued**

ipsilateral striatum (CP) between them. The horizontal axis of the statistical graph represented the CP region of each coronal plane (from rostral to caudal), and the vertical axis represented the intensity of pixels from each coronal plane. The percentage of signal intensity of striatal projection fibers to the total striatal projection fiber signal intensity was used to represent the projection strength to CP at different positions. The gray dashed lines presented the striatum projection center of gravity in each subregion. The bright line represented the average value and the shaded area represented the fluctuation range of the projected signal strength from the caudate putamen of different samples. (E) The correlation coefficient matrix of the mean intensity of pixels originated from the rostral and caudal striatum. The striatal projections were quantified as projection signal volume in each slice normalized by signal volume across the whole CP.  $n = 3$  per group. F, Topography organization between the sensorimotor cortex and the striatum.

**Correlation comparison of input patterns**

To evaluate the input patterns for different types of pyramidal neurons, we conducted Pearson's correlation analysis on the proportion of inputs for IT and PT neurons. The proportion of inputs from most brain regions projecting for these two types of neurons demonstrated high correlation coefficients (above 0.8, Figure S4). These results indicate that the whole-brain input patterns for different types of neurons in the same subregion of the sensorimotor cortex are highly correlated.

Additionally, we constructed a cluster analysis based on the correlation coefficients of the input proportion from the whole brain input regions to reveal related input nuclei.<sup>33,34</sup> This analysis relied on the fact that each injection may cover a subset of neurons, rather than uniformly targeting all neurons of the injected brain region. The input nuclei of IT neurons formed clear multiple clusters (Figures S5A and S5B). Previous studies have reported that bidirectional connections between the motor cortex and motor thalamus are necessary for motor preparations,<sup>35</sup> and the ablation of basal forebrain cholinergic input prevented map reorganization in the primary motor cortex and impaired learning for skilled stretching tasks.<sup>36</sup> These findings indicate that both basal forebrain and motor thalamus input regulates motor cortex function. The diagonal band nucleus (NDB) of the basal forebrain and anteromedial nucleus (AM) inputs for IT neurons in the  $MOp^{IMM}$  and  $MOs^{PMM}$  formed one cluster, and the NDB and AM inputs for the PT neurons in the  $MOp^{ALM}$  were also clustered together (Figures S5A and S5B). Moreover, the NDB and anterodorsal nucleus (AD) inputs for PT neurons in the  $MOs^{AMM}$  and  $MOs^{PMM}$  were also clustered together, which confirms previous reports<sup>33,35</sup> (Figure S5B). Additionally, some input nuclei frequently formed one cluster, such as PO-substantia innominate (SI), olfactory areas (OLF)-SI, the nucleus of reuniens-rhomboid nucleus, the ventral medial nucleus of the thalamus (VM)-the central medial nucleus of the thalamus for IT neurons; ectorhinal area (ECT)-pons, VIS-auditory areas (AUD), cortical subplate-VM for PT neurons (Figures S5A and S5B). Together, these results suggest that cortical pyramidal neurons are heterogeneous and both IT and PT neurons receive input from different combinations of nuclei.

**Brain-wide projection of pyramidal neurons**

We have presented that the pyramidal neurons in the sensorimotor cortex received extensive topographic cortical and subcortical afferents, next we wondered which downstream areas these neurons target. To map the whole-brain projection of IT and PT neurons in different subregions, we injected anterograde Cre-dependent adeno-associated virus (AAV)<sup>10,37</sup> into Fezf2-CreER and PlxnD1-CreER transgenic mice respectively (Figure 4A). The laminar patterns of the labeled neurons verified that these two types of neurons are layer-specific, which is consistent with the brain-wide distributions (Figures 4B and S6). The whole-brain datasets were acquired with the fMOST system and reconstructed to compare the projection pattern of pyramidal neurons in different subregions (Figures S7A and S7B).

IT neurons in the sensorimotor cortex projected mainly to the cortex and striatum on both sides (Figure S8). Therefore, the detailed analysis of the cortical and striatal projection circuit by calculating the fiber signals from each brain slice. To facilitate the comparison of cortical projection patterns of IT neurons in different subregions, the ipsilateral and contralateral projection fibers were calculated and displayed in different colors. The distribution and intensity of the fibers in the ipsilateral and contralateral cortex were highly consistent. Different subregions preferred to dominate the adjacent cortical areas on both sides and showed mirror symmetry across the middle line (Figure S9A). When these subregions were arranged anteriorly and posteriorly according to the location of the injection site, the ipsilateral and contralateral cortical projection centers of the corresponding subregions moved backward continuously (Figures S9B and S9C). In addition, different subregions of the contralateral cortical projection showed layer specificity, evenly distributed in layers 1, 2/3, 5, and 6 (Figure S9D).

The Striatum was organized into distinct regions<sup>38</sup> and associated with different behavioral functions,<sup>39,40</sup> contains at least three functional domains including the sensorimotor, associative, and limbic domains. Among them, the sensorimotor domain approximately corresponds to the dorsolateral striatum or caudoputamen (CP).<sup>38,40–45</sup> The striatal projection circuits in the cortex are mainly derived from IT and PT neurons, and such cell type-specific connections have different functional regulations. Previous studies revealed relatively comprehensive circuit connections between cortical regions and different domains of the striatum but failed to discriminate based on molecularly defined cell types.<sup>38,46</sup> To compare the corticostriatal projections from different subregions of the sensorimotor cortex, we grouped the neurons according to their somata location along the M-L axis. The striatal projection was found to be closely related to the spatial location of neurons (Figure 4C). The ventral domain (CP.v) of the CP received massive inputs from the lateral sites (MOp<sup>ALM</sup> and SSp-ul), while the dorsal part of the CP (CP.d) received massive fibers from the medial sites (MOs<sup>AMM</sup>, MOs<sup>PMM</sup>, MOp<sup>IMM</sup>, and SSp-ll). Specifically, the dorsomedial level of the CP (CP.dm) received dense fibers from the MOs<sup>AMM</sup> and MOs<sup>PMM</sup>, and the dorsolateral (CP.dl) from the MOp<sup>IMM</sup> and SSp-ll which reveals that the different subregions of CP.d integrated distinct parallel pathways from different cortical subregions (Figure 4C). These results reveal that the information flow of the striatum is regulated regularly by projecting from the medial or lateral subregions to the CP.d or CP.v.

We next quantitatively analyzed the striatal projection of IT neurons in different subregions by calculating fiber signal strength from each slice. We found that the projection from different subregions of the sensorimotor subnetwork to the rostral-caudal extent of the CP demonstrated dense and highly overlapping projection fields in the intermediate domain CP (Cpi) (Figure 4D). As the site moved outward, the projection center of gravity shifted toward the caudal CP. We employed correlation analysis for the striatal projections from different subregions and found two lateral subregions (MOp<sup>ALM</sup> and SSp-ul) clustered with high correlation while the other four medial subregions (MOs<sup>AMM</sup>, MOs<sup>PMM</sup>, MOp<sup>IMM</sup>, and SSp-ll) clustered in a different group (Figure 4E). Collectively, these above results illustrate that the sensorimotor subnetwork contains multiple separate striatal projection pathways, and which are closely related to the spatial distribution of the cortical neurons across different subregions (Figure 4F).

For the PT neurons, we found that their axons extended to multiple subcortical brain regions, including the thalamus, midbrain, pons, and medulla oblongata, exhibiting the characteristics of PT neurons. The projection of PT neurons from different subregions showed a regional preference in the targeted thalamus (Figure S10) and superior colliculus (SC) (Figure S11). For the thalamus, the lateral subregions (SSp-ll, MOp<sup>ALM</sup>, SSp-ul) mainly projected to the VENT, while the posterior subregions (MOs<sup>PMM</sup>, SSp-ll) preferentially innervated the dorsolateral thalamic nucleus. The thalamic projection field of MOs<sup>AMM</sup> was the widest, similar to the distribution of its thalamic input. In addition, the VPL received convergent pyramidal projections from the sensory cortices (SSp-ul, SSp-ll), rather than other subregions (Figure S10). For the superior colliculus, we found that the MOs<sup>AMM</sup>, MOs<sup>PMM</sup>, and SSp-ll targeted sublayer a and b of SC, while other subregions preferred the ventrolateral portion (Figure S11). In particular, some PT neurons also exhibited the projection characteristics of IT that project bilaterally in the cortex and to the CP (Figures S7B and S8).

### The whole-brain connection pattern of intratelencephalic and pyramidal tract neurons in different subregions

To further compare the input circuit and projection pattern, we next semi-quantitatively analyzed the long-range connection of PT and IT neurons in the whole brain. As shown in Figure 5, the connection strength of the input circuit and projection was presented in high, medium, and low groups respectively. Different types of pyramidal neurons in the same subregion received similar whole-brain inputs, but different subregions differ significantly. The whole brain projections of the same type of pyramidal neurons in different subregions were different but not as significant as the differences between type-specific neurons.

The whole-brain inputs and projections of PT and IT neurons in the sensorimotor cortex were organized in a spatially dependent topological pattern. For cortical-cortical connections, MOs<sup>AMM</sup> preferred to form strong connections with anterior cortical regions, MOs<sup>PMM</sup> preferred to form connections with posterior regions, and the other four subregions preferred to form connections with intermediate regions. There are strong bidirectional connections between IT neurons in different subregions and specific cortical regions. The PT and IT neurons in different subregions were mainly connected to the striatum by unidirectional connections and showed similar projection patterns. The four medial subregions including MOs<sup>AMM</sup>, MOs<sup>PMM</sup>, MOp<sup>IMM</sup>, and SSp-ll tended to project to the dorsal CP, while the lateral subregions tended to

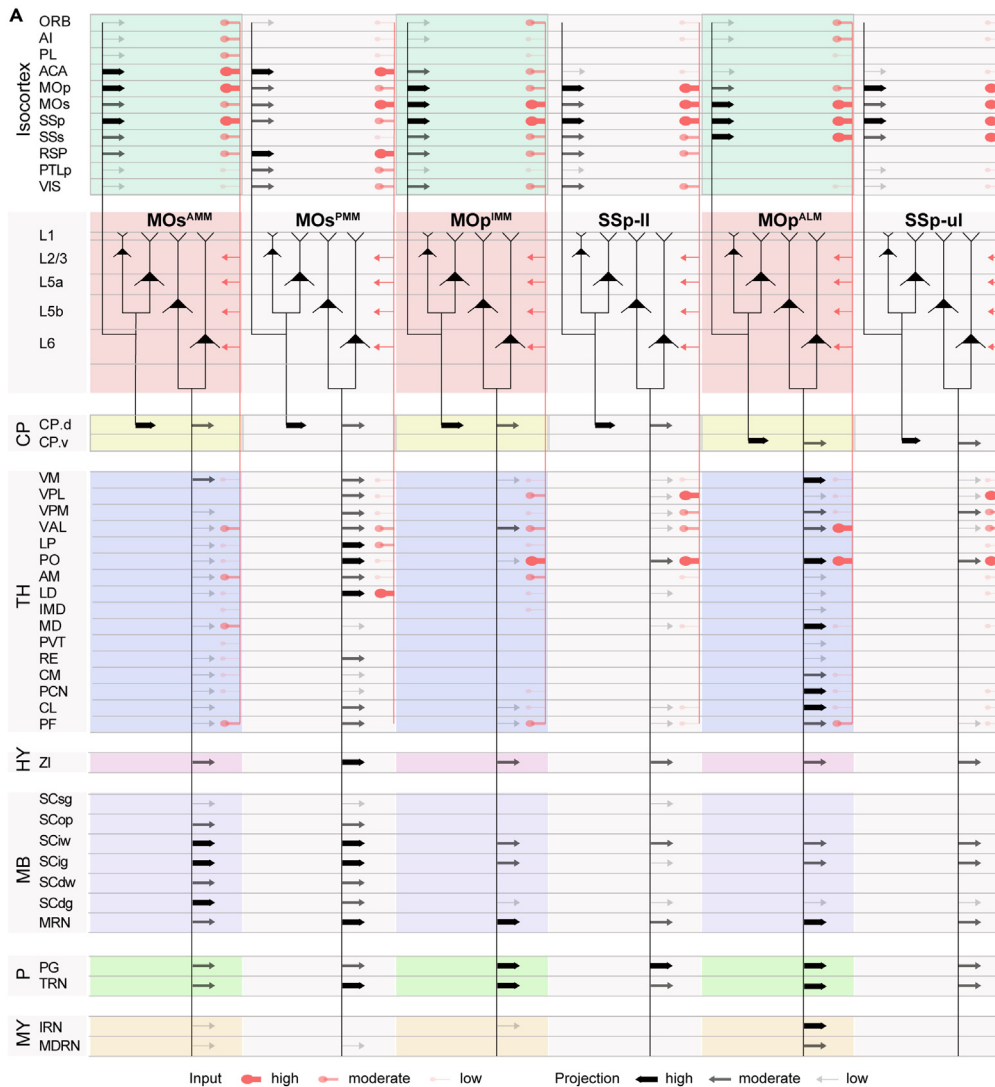


**Figure 5. A wiring diagram of connections between different pyramidal neurons and major cortical regions or subcortical nuclei**

Regardless of input connection strength or output connection strength, this study is expressed as the percentage of the connection density of a single region in the total connection density. The circles indicated the input neurons, and their sizes indicated different connection strengths. Arrows indicated the connection strength of fiber projection, and their thicknesses indicated different connection strengths. The abbreviations of brain regions were provided in Table S1.

project to the ventral CP. PT neurons in different subregions of the sensorimotor cortex form a strong bidirectional network of connections with specific thalamic regions. In addition, connections between PT neurons in the sensorimotor cortex and other subcortical structures including the hypothalamus, midbrain, pons, and medulla were also region-specific (Figure 5). In general, the brain-wide network of PT and IT neurons in different subregions of the sensorimotor cortex is complex and organized according to specific rules.

## DISCUSSION

Combining mouse genetics and viral tracing with the fMOST system, we comprehensively mapped the whole-brain connectivity of pyramidal neurons in six subregions of the sensorimotor cortex. The sensorimotor cortex can be divided into multiple subregions.<sup>3,7,47</sup> Here, we selected six subregions in the primary and secondary motor cortex and sensory cortex with distinct functions.

The  $\text{MOp}^{\text{ALM}}$ ,  $\text{MOs}^{\text{PMM}}$ , and  $\text{MOs}^{\text{AMM}}$  make a great contribution to the control of movement.<sup>3,4</sup> The  $\text{MOp}^{\text{IMM}}$ ,  $\text{SSp-ul}$ , and  $\text{SSp-lI}$ , present different body parts in control of movement.<sup>6,7</sup> While the  $\text{MOp}^{\text{ALM}}$  and  $\text{MOs}^{\text{PMM}}$  contribute to the preparation and learning of movement respectively.<sup>48</sup> These regions work together to coordinate movement with various neuron types and upstream and downstream connections. The whole-brain distribution of the projection targets and the input neurons reveals the distinct spatial distribution patterns of the subregions and layers (Figure 5). The connectivity data provide a framework for understanding how different cortical neuronal types participate in global brain circuits that shape the computations and behavioral functions of the sensorimotor cortex.

Although the retrograde *trans*-synaptic RV tracing system also has some limitations, mainly including two aspects,<sup>49</sup> one is the low labeling efficiency, and the other is that the labeled input neurons may have preferences. However, many parameters were optimized in the existing research method, and the retrograde *trans*-synaptic RV tracing system is currently the main tool for analyzing input circuits,<sup>24</sup> which can reflect the connection between type-specific neurons in objective areas and upstream input neurons. Although the anterograde labeling of axons can reflect the projection pattern of the sensorimotor cortex to a certain extent, the intensity of these projection fibers across the brain regions is overestimated due to the interference of passing fibers.<sup>10</sup> On the other hand, the signal strength of axonal fibers was not necessarily related to the number of synaptic connections. Labeling methods of synaptic connections are more indicative of the strength of connections between different brain regions.<sup>50</sup> Therefore, this tracing method cannot reflect the real connection strength, but reveal the connection circuits between different regions or neurons to a certain extent.

### Topological organization in the upstream circuits of different subregions

According to the anatomical and physiological connections, cortical circuits can be divided into the medial, lateral, and somatic sensorimotor subnetworks, all of which show unique network topologies.<sup>51</sup> The cortico-cortical connections of the subregions followed the proximity rule (Figure 2), that the anterior, posterior, medial, and lateral subregions preferred to receive inputs from the nearby cortices, consistent with the previous research.<sup>10,51</sup> The subcortical input nuclei were mainly in the thalamus with high heterogeneity, which is consistent with previous reports,<sup>10,51</sup> indicating that the thalamus innervates the sensorimotor cortex with different combinations of sub-circuits.<sup>52</sup> However, this study also revealed the thalamic connection network of specific cell types in the sensorimotor cortex. We found that both IT and PT neurons in the same subregion of the sensorimotor cortex received thalamic input from similar regions, but with quantitative differences. Given that PT neurons have much more extensive dendrites in layer 1 and higher-order thalamic areas project to layer 1, it has long been speculated there might be biases in thalamic input.<sup>53</sup> However, no significant difference was found in the thalamic input of IT and PT neurons in this study, especially in the distributed regions of the input neurons. Interestingly, compared with IT neurons, PT neurons in  $\text{MOp}^{\text{IMM}}$  and  $\text{SSp-lI}$  received more thalamic inputs. However, no significant thalamic input connections were found in other subregions, which may be due to the heterogeneity of neurons in different regions, further demonstrating the importance of detailed cell-type anatomy across regions.

Different layers of the same cortical area have distinct roles in information integration. The secondary motor cortex preferentially projected to the deep layer of the primary motor cortex, and likewise sensory thalamus and frontal cortex.<sup>54</sup> These findings coincided with our results, that  $\text{MOs}^{\text{AMM}}$ , PO, PF, AM, and PCN target the PT neurons (Figures 1, 2, 3, and S5). The existence of other differentiated input nuclei suggests that there may be other sub-circuits in the motor cortex, which provide references for the study of other structural and functional circuits. Combining the input distribution of different subregions and neuronal types with other known connectivity studies of the sensorimotor cortex,<sup>22,23</sup> we verified that the input patterns of cortical neurons in different subregions are different while the input distributions of different pyramidal neurons in the same subregion are similar.

### Topologically organized cortico-striatal circuits

The sensorimotor domain is approximately projected to the dorsolateral striatum, consistent with previous findings.<sup>10,40–45</sup> In addition, the results showed no overlapping in the striatal projection of PT and IT neurons in the sensorimotor cortex, especially  $\text{MOp}^{\text{IMM}}$  (Figure S8). Prior studies with chemical tracers and no cell type information have implicitly interpreted this differently,<sup>46</sup> whereas it is known from single axon reconstructions that cell type differences probably exist. Although

undersampled with sparse reconstructions, this study still suggests that there are real differences between IT neurons and PT neurons.<sup>55</sup> This further illustrates the importance of type-specific circuit connections.

The striatal projections from different subregions within the sensorimotor subnetwork displayed a topographic organization, consistent with the results of previous studies employing chemical tracers.<sup>38,46</sup> However, different from those reports, this study revealed the striatum projection circuit of specific cell types by employing transgenic mice and found that the projection paths of IT and PT neurons were separated, further verifying the previous speculation that the connections of different neurons were unique.<sup>55</sup> Specifically, the projection output of IT neurons from different regions in MOp was not overlapping, to different parts of CP. This indicates that at least two or more groups of IT neurons in MOp regulate the CP and thus perform different functions.<sup>40,56</sup> In addition, the MOs<sup>AMM</sup>, MOs<sup>PMM</sup>, MOp<sup>IMM</sup>, and SSp-II preferentially projected to the anterior part of the striatum, while the MOp<sup>ALM</sup> and SSp-ul preferentially projected to the posterior part of the striatum. These results are different from the known research, in which IT neurons in layer 5 of the sensory area preferred to project to the anterior part of the striatum, while the motor area preferred to project to the posterior part of the striatum.<sup>37</sup> Together, these differences in the striatal projection might originate from different injection sites or cell types. Although the axon fibers of some PT neurons terminate in the striatum, there are some axons that pass through the striatum and reach other nuclei under the cortex. Therefore, a large number of passing fibers will seriously interfere with the calculation of signal strength from axon fiber, resulting in low accuracy of the results. In the future, the striatal projection pattern of PT neurons can be explored by the axonal reconstruction of single neurons or synaptic labeling.

### Limitations of the study

Although the method used in this study is a commonly used tool for tracing neural circuits in the field of neurobiology, it has some limitations, including low labeling efficiency, possible labeling preferences for specific brain regions or cell types, and it cannot truly reflect the connection strength of the neural network.

### STAR★METHODS

Detailed methods are provided in the online version of this paper and include the following:

- KEY RESOURCES TABLE
- RESOURCE AVAILABILITY
  - Lead contact
  - Materials availability
  - Data and code availability
- EXPERIMENTAL MODEL AND SUBJECT DETAILS
  - Animals
- METHOD DETAILS
  - Stereotactic injection of virus
  - Perfusion and resin embedding
  - Imaging
  - Visualization and reconstruction
- QUANTIFICATION AND STATISTICAL ANALYSIS

### SUPPLEMENTAL INFORMATION

Supplemental information can be found online at <https://doi.org/10.1016/j.isci.2023.106316>.

### ACKNOWLEDGMENTS

We thank Xueyan Jia, Yang Yang, Jianping Zhang, Peilin Zhao, and Pan Luo for their help with experiments and data analysis. We acknowledge support from the STI2030-Major Projects (2021ZD0201001, 2021ZD0201002), National Nature Science Foundation of China (Nos. 61890953 and 31871088) and CAMS Innovation Fund for Medical Sciences (No. 2019-I2M-5-014). We also thank the Britton Chance Center of Biomedical Photonics for technical assistance.

## AUTHOR CONTRIBUTIONS

X.L. and H.G. conceived and designed the study. M.Y., A.T., and Q.S. optimized viral tracing and analyzed the data. X.A. and J.H. provided the animals. T.J. and A.L. performed whole-brain imaging and processing. X.L., H.G., M.Y., A.T., and J.H. wrote and modified the article.

## DECLARATION OF INTERESTS

The authors declare no competing interests.

## INCLUSION AND DIVERSITY

We support inclusive, diverse, and equitable conduct of research.

Received: November 10, 2022

Revised: December 19, 2022

Accepted: February 27, 2023

Published: March 2, 2023

## REFERENCES

- Abbott, L.F., Bock, D.D., Callaway, E.M., Denk, W., Dulac, C., Fairhall, A.L., Fiete, I., Harris, K.M., Helmstaedter, M., Jain, V., et al. (2020). The mind of a mouse. *Cell* 182, 1372–1376. <https://doi.org/10.1016/j.cell.2020.08.010>.
- Hira, R., Ohkubo, F., Ozawa, K., Isomura, Y., Kitamura, K., Kano, M., Kasai, H., and Matsuzaki, M. (2013). Spatiotemporal dynamics of functional clusters of neurons in the mouse motor cortex during a voluntary movement. *J. Neurosci.* 33, 1377–1390. <https://doi.org/10.1523/JNEUROSCI.2550-12.2013>.
- Harrison, T.C., Ayling, O.G.S., and Murphy, T.H. (2012). Distinct cortical circuit mechanisms for complex forelimb movement and motor map Topography. *Neuron* 74, 397–409.
- Barthas, F., and Kwan, A.C. (2017). Secondary motor cortex: where ‘sensory’ meets ‘motor’ in the rodent frontal cortex. *Trends Neurosci.* 40, 181–193. <https://doi.org/10.1016/j.tins.2016.11.006>.
- Hira, R., Terada, S.I., Kondo, M., and Matsuzaki, M. (2015). Distinct functional modules for discrete and rhythmic forelimb movements in the mouse motor cortex. *J. Neurosci.* 35, 13311–13322. <https://doi.org/10.1523/JNEUROSCI.2731-15.2015>.
- Mathis, M.W., Mathis, A., and Uchida, N. (2017). Somatosensory cortex plays an essential role in forelimb motor adaptation in mice. *Neuron* 93, 1493–1503.e6.
- Tennant, K.A., Adkins, D.L., Donlan, N.A., Asay, A.L., Thomas, N., Kleim, J.A., and Jones, T.A. (2011). The organization of the forelimb representation of the C57BL/6 mouse motor cortex as defined by intracortical microstimulation and cytoarchitecture. *Cerebr. Cortex* 21, 865–876. <https://doi.org/10.1093/cercor/bhq159>.
- Peng, H., Xie, P., Liu, L., Kuang, X., Wang, Y., Qu, L., Gong, H., Jiang, S., Li, A., Ruan, Z., et al. (2021). Morphological diversity of single neurons in molecularly defined cell types. *Nature* 598, 174–181. <https://doi.org/10.1038/s41586-021-03941-1>.
- Muñoz-Castañeda, R., Zingg, B., Matho, K.S., Chen, X., Wang, Q., Foster, N.N., Li, A., Narasimhan, A., Hirokawa, K.E., Huo, B., et al. (2021). Cellular anatomy of the mouse primary motor cortex. *Nature* 598, 159–166. <https://doi.org/10.1038/s41586-021-03970-w>.
- Harris, J.A., Mihalas, S., Hirokawa, K.E., Whitesell, J.D., Choi, H., Bernard, A., Bohn, P., Caldejon, S., Casal, L., Cho, A., et al. (2019). Hierarchical organization of cortical and thalamic connectivity. *Nature* 575, 195–202. <https://doi.org/10.1038/s41586-019-1716-z>.
- Li, X., Yu, B., Sun, Q., Zhang, Y., Ren, M., Zhang, X., Li, A., Yuan, J., Madisen, L., Luo, Q., et al. (2018). Generation of a whole-brain atlas for the cholinergic system and mesoscopic projectome analysis of basal forebrain cholinergic neurons. *Proc. Natl. Acad. Sci. USA* 115, 415–420. <https://doi.org/10.1073/pnas.1703601115>.
- Currie, S.P., Ammer, J.J., Premchand, B., Dacre, J., Wu, Y., Eleftheriou, C., Colligan, M., Clarke, T., Mitchell, L., Faisal, A.A., et al. (2022). Movement-specific signaling is differentially distributed across motor cortex layer 5 projection neuron classes. *Cell Rep.* 39, 110801. <https://doi.org/10.1016/j.celrep.2022.110801>.
- Economo, M.N., Viswanathan, S., Tasic, B., Bas, E., Winnubst, J., Menon, V., Graybiel, L.T., Nguyen, T.N., Smith, K.A., Yao, Z., et al. (2018). Distinct descending motor cortex pathways and their roles in movement. *Nature* 563, 79–84. <https://doi.org/10.1038/s41586-018-0642-9>.
- Chen, T.W., Li, N., Daie, K., and Svoboda, K. (2017). A map of anticipatory activity in mouse motor cortex. *Neuron* 94, 866–879.e4. <https://doi.org/10.1016/j.neuron.2017.05.005>.
- Levy, S., Lavzin, M., Benisty, H., Ghanayim, A., Dubin, U., Achvat, S., Brosh, Z., Aeed, F., Mensh, B.D., Schiller, Y., et al. (2020). Cell-type-specific outcome representation in the primary motor cortex. *Neuron* 107, 954–971.e9. <https://doi.org/10.1016/j.neuron.2020.06.006>.
- Komiyama, T., Sato, T.R., O’Connor, D.H., Zhang, Y.X., Huber, D., Hooks, B.M., Gabitto, M., and Svoboda, K. (2010). Learning-related fine-scale specificity imaged in motor cortex circuits of behaving mice. *Nature* 464, 1182–1186. <https://doi.org/10.1038/nature08897>.
- Park, J., Phillips, J.W., Guo, J.Z., Martin, K.A., Hantman, A.W., and Dudman, J.T. (2022). Motor cortical output for skilled forelimb movement is selectively distributed across projection neuron classes. *Sci. Adv.* 8, eabj5167.
- Currie, S.P., Ammer, J.J., Premchand, B., Dacre, J., Wu, Y., Eleftheriou, C., Colligan, M., Clarke, T., Mitchell, L., Faisal, A.A., et al. (2022). Movement-specific signaling is differentially distributed across motor cortex layer 5 projection neuron classes. *Cell Rep.* 39, 110801.
- Wang, Y., and Kurata, K. (1998). Quantitative analyses of thalamic and cortical origins of neurons projecting to the rostral and caudal forelimb motor areas in the cerebral cortex of rats. *Brain Res.* 781, 137–147.
- Zingg, B., Hintiryan, H., Gou, L., Song, M.Y., Bay, M., Bienkowski, M.S., Foster, N.N., Yamashita, S., Bowman, I., Toga, A.W., and Dong, H.W. (2014). Neural networks of the mouse neocortex. *Cell* 156, 1096–1111. <https://doi.org/10.1016/j.cell.2014.02.023>.
- Yokoi, A., and Diedrichsen, J. (2019). Neural organization of hierarchical motor sequence representations in the human neocortex. *Neuron* 103, 1178–1190.e7. <https://doi.org/10.1016/j.neuron.2019.06.017>.
- Duan, Z., Li, A., Gong, H., and Li, X. (2020). A whole-brain map of long-range inputs to GABAergic interneurons in the mouse caudal forelimb area. *Neurosci. Bull.* 36,

- 493–505. <https://doi.org/10.1007/s12264-019-00458-6>.
23. Luo, P., Li, A., Zheng, Y., Han, Y., Tian, J., Xu, Z., Gong, H., and Li, X. (2019). Whole brain mapping of long-range direct input to glutamatergic and GABAergic neurons in motor cortex. *Front. Neuroanat.* 13, 44. <https://doi.org/10.3389/fnana.2019.00044>.
  24. Wickersham, I.R., Lyon, D.C., Barnard, R.J.O., Mori, T., Finke, S., Conzelmann, K.K., Young, J.A.T., and Callaway, E.M. (2007). Monosynaptic restriction of transsynaptic tracing from single, genetically targeted neurons. *Neuron* 53, 639–647. <https://doi.org/10.1016/j.neuron.2007.01.033>.
  25. Sun, Q., Li, X., Ren, M., Zhao, M., Zhong, Q., Ren, Y., Luo, P., Ni, H., Zhang, X., Zhang, C., et al. (2019). A whole-brain map of long-range inputs to GABAergic interneurons in the mouse medial prefrontal cortex. *Nat. Neurosci.* 22, 1357–1370. <https://doi.org/10.1038/s41593-019-0429-9>.
  26. Yang, Y., Jiang, T., Jia, X., Yuan, J., Li, X., and Gong, H. (2022). Whole-brain connectome of GABAergic neurons in the mouse zona incerta. *Neurosci. Bull.* 38, 1315–1329. <https://doi.org/10.1007/s12264-022-00930-w>.
  27. Gong, H., Xu, D., Yuan, J., Li, X., Guo, C., Peng, J., Li, Y., Schwarz, L.A., Li, A., Hu, B., et al. (2016). High-throughput dual-colour precision imaging for brain-wide connectome with cytoarchitectonic landmarks at the cellular level. *Nat. Commun.* 7, 12142. <https://doi.org/10.1038/ncomms12142>.
  28. Wickersham, I.R., Lyon, D.C., Barnard, R.J.O., Mori, T., Finke, S., Conzelmann, K.-K., Young, J.A.T., and Callaway, E.M. (2007). Monosynaptic restriction of transsynaptic tracing from single, genetically targeted neurons. *Neuron* 53, 639–647.
  29. Matho, K.S., Huilgol, D., Galbavy, W., He, M., Kim, G., An, X., Lu, J., Wu, P., Di Bella, D.J., Shetty, A.S., et al. (2021). Genetic dissection of the glutamatergic neuron system in cerebral cortex. *Nature* 598, 182–187. <https://doi.org/10.1038/s41586-021-03955-9>.
  30. Peng, J., Long, B., Yuan, J., Peng, X., Ni, H., Li, X., Gong, H., Luo, Q., and Li, A. (2017). A quantitative analysis of the distribution of CRH neurons in whole mouse brain. *Front. Neuroanat.* 11, 63. <https://doi.org/10.3389/fnana.2017.00063>.
  31. Huo, Y., Chen, H., and Guo, Z.V. (2020). Mapping functional connectivity from the dorsal cortex to the thalamus. *Neuron* 107, 1080–1094.e5. <https://doi.org/10.1016/j.neuron.2020.06.038>.
  32. Van der Werf, Y.D., Witter, M.P., and Groenewegen, H.J. (2002). The intralaminar and midline nuclei of the thalamus. Anatomical and functional evidence for participation in processes of arousal and awareness. *Brain Res. Brain Res. Rev.* 39, 107–140. [https://doi.org/10.1016/s0165-0173\(02\)00181-9](https://doi.org/10.1016/s0165-0173(02)00181-9).
  33. Menegas, W., Bergan, J.F., Ogawa, S.K., Isogai, Y., Umadevi Venkataraju, K., Osten, P., Uchida, N., and Watabe-Uchida, M. (2015). Dopamine neurons projecting to the posterior striatum form an anatomically distinct subclass. *Elife* 4, e10032. <https://doi.org/10.7554/eLife.10032>.
  34. Weissbourd, B., Ren, J., DeLoach, K.E., Guenther, C.J., Miyamichi, K., and Luo, L. (2014). Presynaptic partners of dorsal raphe serotonergic and GABAergic neurons. *Neuron* 83, 645–662.
  35. Guo, Z.V., Inagaki, H.K., Daie, K., Druckmann, S., Gerfen, C.R., and Svoboda, K. (2017). Maintenance of persistent activity in a frontal thalamocortical loop. *Nature* 545, 181–186. <https://doi.org/10.1038/nature22324>.
  36. Conner, J.M., Culberson, A., Packowski, C., Chiba, A.A., and Tuszynski, M.H. (2003). Lesions of the basal forebrain cholinergic system impair task acquisition and abolish cortical plasticity associated with motor skill learning. *Neuron* 38, 819–829.
  37. Hooks, B.M., Papale, A.E., Paletzki, R.F., Feroze, M.W., Eastwood, B.S., Couey, J.J., Winnubst, J., Chandrashekar, J., and Gerfen, C.R. (2018). Topographic precision in sensory and motor corticostriatal projections varies across cell type and cortical area. *Nat. Commun.* 9, 3549. <https://doi.org/10.1038/s41467-018-05780-7>.
  38. Hintiryan, H., Foster, N.N., Bowman, I., Bay, M., Song, M.Y., Gou, L., Yamashita, S., Bienkowski, M.S., Zingg, B., Zhu, M., et al. (2016). The mouse cortico-striatal projectome. *Nat. Neurosci.* 19, 1100–1114. <https://doi.org/10.1038/nn.4332>.
  39. Gremel, C.M., and Costa, R.M. (2013). Orbitofrontal and striatal circuits dynamically encode the shift between goal-directed and habitual actions. *Nat. Commun.* 4, 2264. <https://doi.org/10.1038/ncomms3264>.
  40. Yin, H.H., and Knowlton, B.J. (2006). The role of the basal ganglia in habit formation. *Nat. Rev. Neurosci.* 7, 464–476. <https://doi.org/10.1038/nrn1919>.
  41. Gruber, A.J., and McDonald, R.J. (2012). Context, emotion, and the strategic pursuit of goals: interactions among multiple brain systems controlling motivated behavior. *Front. Behav. Neurosci.* 6, 50. <https://doi.org/10.3389/fnbeh.2012.00050>.
  42. Thorn, C.A., Atallah, H., Howe, M., and Graybiel, A.M. (2010). Differential dynamics of activity changes in dorsolateral and dorsomedial striatal loops during learning. *Neuron* 66, 781–795. <https://doi.org/10.1016/j.neuron.2010.04.036>.
  43. Belin, D., Jonkman, S., Dickinson, A., Robbins, T.W., and Everitt, B.J. (2009). Parallel and interactive learning processes within the basal ganglia: relevance for the understanding of addiction. *Behav. Brain Res.* 199, 89–102. <https://doi.org/10.1016/j.bbr.2008.09.027>.
  44. Balleine, B.W., Liljeholm, M., and Ostlund, S.B. (2009). The integrative function of the basal ganglia in instrumental conditioning. *Behav. Brain Res.* 199, 43–52. <https://doi.org/10.1016/j.bbr.2008.10.034>.
  45. Yin, H.H., Ostlund, S.B., Knowlton, B.J., and Balleine, B.W. (2005). The role of the dorsomedial striatum in instrumental conditioning. *Eur. J. Neurosci.* 22, 513–523. <https://doi.org/10.1111/j.1460-9568.2005.04218.x>.
  46. Hunnicutt, B.J., Jongbloets, B.C., Birdsong, W.T., Gertz, K.J., Zhong, H., and Mao, T. (2016). A comprehensive excitatory input map of the striatum reveals novel functional organization. *Elife* 5, e19103. <https://doi.org/10.7554/eLife.19103>.
  47. Barth, T.M., Jones, T.A., and Schallert, T. (1990). Functional subdivisions of the rat somatic sensorimotor cortex. *Behav. Brain Res.* 39, 73–95.
  48. Sauerbrei, B.A., Guo, J.Z., Cohen, J.D., Mischiat, M., Guo, W., Kabra, M., Verma, N., Mensh, B., Branson, K., and Hantman, A.W. (2020). Cortical pattern generation during dexterous movement is input-driven. *Nature* 577, 386–391. <https://doi.org/10.1038/s41586-019-1869-9>.
  49. Alexandra, R., and Beier, K.T. (2020). Can transsynaptic viral strategies be used to reveal functional aspects of neural circuitry? *J. Neurosci. Methods* 348, 109005.
  50. Liu, Q., Wu, Y., Wang, H., Jia, F., and Xu, F. (2022). Viral tools for neural circuit tracing. *Neurosci. Bull.* 38, 1508–1518. <https://doi.org/10.1007/s12264-022-00949-z>.
  51. Oh, S.W., Harris, J.A., Ng, L., Winslow, B., Cain, N., Mihalas, S., Wang, Q., Lau, C., Kuan, L., Henry, A.M., et al. (2014). A mesoscale connectome of the mouse brain. *Nature* 508, 207–214. <https://doi.org/10.1038/nature13186>.
  52. Hunnicutt, B.J., Long, B.R., Kusefoglou, D., Gertz, K.J., Zhong, H., and Mao, T. (2014). A comprehensive thalamocortical projection map at the mesoscopic level. *Nat. Neurosci.* 17, 1276–1285. <https://doi.org/10.1038/nn.3780>.
  53. Phillips, J.W., Schulmann, A., Hara, E., Winnubst, J., Liu, C., Valakh, V., Wang, L., Shields, B.C., Korff, W., Chandrashekar, J., et al. (2019). A repeated molecular architecture across thalamic pathways. *Nat. Neurosci.* 22, 1925–1935. <https://doi.org/10.1038/s41593-019-0483-3>.
  54. Hooks, B.M., Mao, T., Gutnisky, D.A., Yamawaki, N., Svoboda, K., and Shepherd, G.M.G. (2013). Organization of cortical and thalamic input to pyramidal neurons in mouse motor cortex. *J. Neurosci.* 33, 748–760. <https://doi.org/10.1523/JNEUROSCI.4338-12.2013>.
  55. Winnubst, J., Bas, E., Ferreira, T.A., Wu, Z., Economo, M.N., Edson, P., Arthur, B.J., Bruns, C., Rokicki, K., Schauder, D., et al. (2019). Reconstruction of 1,000 projection neurons reveals new cell types and organization of long-range connectivity in the mouse brain. *Cell* 179, 268–281.e13. <https://doi.org/10.1016/j.cell.2019.07.042>.
  56. dos Santos, L.M., Boschen, S.L., Bortolanza, M., de Oliveira, W.F., Furigo, I.C., Mota-Ortiz, S.R., Da Cunha, C., and Canteras, N.S. (2012).

- The role of the ventrolateral caudoputamen in predatory hunting. *Physiol. Behav.* 105, 893–898. <https://doi.org/10.1016/j.physbeh.2011.10.021>.
57. Xu, Z., Feng, Z., Zhao, M., Sun, Q., Deng, L., Jia, X., Jiang, T., Luo, P., Chen, W., Tudi, A., et al. (2021). Whole-brain connectivity atlas of glutamatergic and GABAergic neurons in the mouse dorsal and median raphe nuclei. *Elife* 10, e65502. <https://doi.org/10.7554/eLife.65502>.
58. Hafner, G., Witte, M., Guy, J., Subhashini, N., Fenno, L.E., Ramakrishnan, C., Kim, Y.S., Deisseroth, K., Callaway, E.M., Oberhuber, M., et al. (2019). Mapping brain-wide afferent inputs of parvalbumin-expressing GABAergic neurons in barrel cortex reveals local and long-range circuit motifs. *Cell Rep.* 28, 3450–3461.e8. <https://doi.org/10.1016/j.celrep.2019.08.064>.
59. Gielow, M.R., and Zaborszky, L. (2017). The input-output relationship of the cholinergic basal forebrain. *Cell Rep.* 18, 1817–1830. <https://doi.org/10.1016/j.celrep.2017.01.060>.
60. Faget, L., Osakada, F., Duan, J., Ressler, R., Johnson, A.B., Proudfoot, J.A., Yoo, J.H., Callaway, E.M., and Hnasko, T.S. (2016). Afferent inputs to neurotransmitter-defined cell types in the ventral tegmental area. *Cell Rep.* 15, 2796–2808. <https://doi.org/10.1016/j.celrep.2016.05.057>.
61. Ren, M., Tian, J., Sun, Q., Chen, S., Luo, T., Jia, X., Jiang, T., Luo, Q., Gong, H., and Li, X. (2021). Plastic embedding for precise imaging of large-scale biological tissues labeled with multiple fluorescent dyes and proteins. *Biomed. Opt Express* 12, 6730–6745. <https://doi.org/10.1364/BOE.435120>.
62. Kuan, L., Li, Y., Lau, C., Feng, D., Bernard, A., Sunkin, S.M., Zeng, H., Dang, C., Hawrylycz, M., and Ng, L. (2015). Neuroinformatics of the allen mouse brain connectivity atlas. *Methods* 73, 4–17.

## STAR★METHODS

### KEY RESOURCES TABLE

REAGENT or RESOURCE	SOURCE	IDENTIFIER
Pentobarbital sodium	Sigma-Aldrich	11715
Tamoxifen	Sigma-Aldrich	T5648
Corn oil	Aladdin	C116025
Phosphate buffered saline (PBS)	Sigma-Aldrich	P4417
Paraformaldehyde (PFA)	Sigma-Aldrich	158127
Glycol methacrylate (GMA) resin	Ted Pella	N/A

### RESOURCE AVAILABILITY

#### Lead contact

Further information and requests for resources and reagents should be directed to and will be fulfilled by the corresponding author, Xiangning Li ([lixiangning@mail.hust.edu.cn](mailto:lixiangning@mail.hust.edu.cn)).

#### Materials availability

This study did not generate new unique reagents.

#### Data and code availability

Data reported in this paper will be shared by the [lead contact](#) upon request. All custom-made codes or any additional information required to reanalyze the data reported in this paper is available from the [lead contact](#) upon request.

## EXPERIMENTAL MODEL AND SUBJECT DETAILS

### Animals

We used 2–6 months old male PlxnD1-2A-CreER and Fezf2-2A-CreER<sup>29</sup> (a gift from Josh Huang's laboratory, Cold Spring Harbor Lab) to combine viral tracing to specifically label IT and PT neurons in the sensorimotor cortex. In addition, we crossed PlxnD1-2A-CreER or Fezf2-2A-CreER mouse with Ai3 mouse (purchased from The Jackson Laboratory) to verify the specificity of labeled neurons. All mice were kept in a suitable environment with sufficient water and food, and animal experiments were conducted in accordance with the requirements of the Animal Ethics Committee of Huazhong University of Science and Technology.

## METHOD DETAILS

### Stereotactic injection of virus

We used a syringe to draw anesthetics (1% pentobarbital sodium in 0.9% saline) into the mouse intraperitoneally (0.1 mL anesthetic per 10g bodyweight, 0.1 mL/10 g) and waited for their deep anesthesia. The state of anesthesia by gently pricking the hind foot of mice with a syringe needle and observing whether the mice produced a limb retraction response. We fixed the mouse on the adapter, cut the skin, and exposed the skull. Then, we adjusted the balance and determined the target site. After that, we gently drilled a small hole with an electric drill, and the virus was propelled to the target depth using a pressure injection pump (Nanoject II: Drummond Scientific, Co., Broomall, PA, United States). In our research, we mainly used specific transgenic mice combined with viruses to target connection circuits of specific types of neurons. For studying input connectivity, we injected AAV-Helper (helper adeno-associated virus mixture (mixed with rAAV2/9-Ef1 $\alpha$ -DIO-mCherry-2a-TVA-WPRE-pA and rAAV2/9-Ef1 $\alpha$ -DIO-RG-WPRE-pA as the ratio of 1: 2, Titer: 2.00E + 12 vg/ml)) and RV virus (RV- $\Delta$ G-EnvA-EGFP (2.00E + 8 IFU/ml)) in CreER mouse.<sup>57–60</sup> These above viruses were purchased from BrainVTA. We injected rAAV9-CAG-DIO-EGFP virus (UNC Viral Core) in CreER mice to trace the projection. The sensorimotor cortex contains the stereotactic coordinates used for injection, such as MOp<sup>ALM</sup> (AP: +1.5, ML: -2), MOs<sup>AMM</sup> (AP: +1.5, ML: -0.6), MOp<sup>IMM</sup> (AP: +0.37, ML: -1.1), SSp-ul (AP: -0.01, ML: 2.46), SSp-II (AP: -0.79, ML: -1.75) and MOs<sup>PMM</sup> (AP: -1.5, ML: -0.75). All mice were intraperitoneally injected with Tamoxifen (Sigma-Aldrich,

T5648) at a concentration of 20 mg/mL on the third day after the initial virus injection. The Tamoxifen solution was formulated with 20 mg of Tamoxifen dissolved in 1 ml of corn oil (Aladdin, C116025).

### Perfusion and resin embedding

Mice were anesthetized with an anesthetic, and the heart was perfused with 0.01M PBS (Sigma-Aldrich Inc., St Louis, MO, USA) and 4% paraformaldehyde (PFA, Sigma-Aldrich Inc., St Louis, MO, USA). The brain was extracted and placed overnight in 4% PFA, and then rinsed with 0.01M PBS overnight. Then, all samples were rinsed overnight in 0.01M PBS. Among the few samples, we used the vibration section (Leica VT1200) to obtain 50  $\mu\text{m}$  brain slices for the observation of initial cells and detection of preliminary results, including the range of infection at the injection site and the efficiency of viral labeling. Most of the other samples were embedded with GMA resin<sup>11,61</sup> and imaged by the fMOST system for obtaining whole-brain connectivity atlas. Simply, the samples were dehydrated in gradient alcohol (50, 70, and 95% ethanol in 4 °C environments), replaced every hour. Then soaked the sample in a gradient of glycol methacrylate (GMA, Ted Pella, Inc., Redding, CA, The United States), 70, 85, and 100% concentration of GMA, soaked for 2 hours each, followed by immersion in 100% GMA, overnight at 4 °C, and then immersed in GMA prepolymer solution for 3 days to fully penetrate. Finally, the samples were placed in a vacuum oven at 48 °C for 24 hours for polymerization.

### Imaging

The continuous sections were obtained by vibrating microtome. Then, the brain slices were placed in the orifice and incubated with diluted DAPI or PI solution for 5 min and rinsed 3-5 times with 0.01M PBS. After that, these brain slices were immobilized by confocal microscopy (Zeiss LSM710) to observe the labeled signals and cytoarchitectural information. Finally, based on cytoarchitecture and referring to the CCF to determine the area where the neuron or fiber signal is located.

For whole-brain imaging, the sample was embedded by GMA resin, and automatically sliced and continuously imaged using the fMOST system.<sup>27</sup> By moving the stage, the lens imaged the entire plane of the sample in a mosaic manner. Subsequently, the diamond knife removed the imaged section of the sample, and then imaged on the surface again. After many cycles, until all the mouse brain was imaged, a complete and continuous mouse brain dataset could be obtained, with a voxel resolution of 0.32  $\mu\text{m}$   $\times$  0.32  $\mu\text{m}$   $\times$  2  $\mu\text{m}$ .

### Visualization and reconstruction

For the collected high-resolution data set, we first preprocessed the image to correct the uneven illumination and eliminate background noise,<sup>27</sup> and then registered the image to the CCF based on a high-level grayscale registration algorithm registration,<sup>62</sup> and extracted the neuron and fiber signals to obtain SWC files and continuous TIFF format pictures. After that, we import the calculated datasets or image into Amira software (v5.2.2, Mercury Computer Systems, San Diego, CA, United States), and render the three-dimensional image with different colors.

### QUANTIFICATION AND STATISTICAL ANALYSIS

For input neurons, we firstly used NeuroGPS to automatically identify and locate the somata of these neurons. Then, we manually examined all neurons in the upstream input areas to avoid unrecognized errors and registered the coordinates of these neurons to CCF. The neurons at the injection site were eliminated, and the input neurons from other different regions were combined together, which was called the total input neurons. In order to reflect the connection strength of different input regions to the injection site, the percentage of input neurons in a single region to the total input neurons was presented in this study. Subsequent analyses were based on the connection strength values of different brain regions. The cluster analysis of the whole brain input nuclei to pyramidal neurons in different subregions was based on GraphPad Prism v.8.02 software and SPSS software (v22, IBM, New York, United States). First, employing GraphPad Prism v.8.02 software to calculate the correlation coefficients between the input proportion of different regions. Then, the obtained correlation coefficients were imported into SPSS software for systematic clustering. Finally, the correlation coefficients of different input regions were sorted in GraphPad Prism v.8.02 software according to the classification, and matrix diagrams were drawn. The two-tailed Student's t-test and one-way ANOVA followed by Tukey's post hoc tests were performed by Graphpad Prism v.8.02.

As for the projection data, we employed the same method to calculate the whole brain projection of pyramidal neurons.<sup>57</sup> Briefly, a continuous whole-brain dataset was downsampled to a voxel resolution of  $10 \mu\text{m}^3$  and then registered with CCF. Then the datasets were segmented and binarized to extract the labeled signals. Next, we compared the extracted signals with the original data to remove the noise information. Finally, we obtain the signal points of data blocks at the volume of  $1 \mu\text{m} \times 1 \mu\text{m} \times 1 \mu\text{m}$  and applied them to the whole brain datasets for obtaining the projection signals of different brain regions.